



Originally published as:

Di Giacomo, D., Parolai, S., Bormann, P., Grosser, H., Saul, J., Wang, R., Zschau, J. (2010): Suitability of rapid energy magnitude determinations for emergency response purposes. - *Geophysical Journal International*, 180, 1, pp. 361—374.

DOI: <http://doi.org/10.1111/j.1365-246X.2009.04416.x>

## Suitability of rapid energy magnitude determinations for emergency response purposes

Domenico Di Giacomo,<sup>1,2</sup> Stefano Parolai,<sup>1</sup> Peter Bormann,<sup>1</sup> Helmut Grosser,<sup>1</sup> Joachim Saul,<sup>1</sup> Rongjiang Wang<sup>1</sup> and Jochen Zschau<sup>1</sup>

<sup>1</sup>Helmholtz Centre Potsdam GFZ German Research Centre for Geosciences, Telegrafenberg D-14473 Potsdam, Germany. E-mail: domenico@gfz-potsdam.de

<sup>2</sup>Institute of Geosciences, Karl-Liebknecht-Str., 14476 Potsdam, Germany

Accepted 2009 October 9. Received 2009 July 30; in original form 2009 March 30

### SUMMARY

It is common practice in the seismological community to use, especially for large earthquakes, the moment magnitude  $M_w$  as a unique magnitude parameter to evaluate the earthquake's damage potential. However, as a static measure of earthquake size,  $M_w$  does not provide direct information about the released seismic wave energy and its high frequency content, which is the more interesting information both for engineering purposes and for a rapid assessment of the earthquake's shaking potential. Therefore, we recommend to provide to disaster management organizations besides  $M_w$  also sufficiently accurate energy magnitude determinations as soon as possible after large earthquakes. We developed and extensively tested a rapid method for calculating the energy magnitude  $M_e$  within about 10–15 min after an earthquake's occurrence. The method is based on pre-calculated spectral amplitude decay functions obtained from numerical simulations of Green's functions. After empirical validation, the procedure has been applied offline to a large data set of 767 shallow earthquakes that have been grouped according to their type of mechanism (strike-slip, normal faulting, thrust faulting, etc.). The suitability of the proposed approach is discussed by comparing our rapid  $M_e$  estimates with  $M_w$  published by GCMT as well as with  $M_w$  and  $M_e$  reported by the USGS.  $M_w$  is on average slightly larger than our  $M_e$  for all types of mechanisms. No clear dependence on source mechanism is observed for our  $M_e$  estimates. In contrast,  $M_e$  from the USGS is generally larger than  $M_w$  for strike-slip earthquakes and generally smaller for the other source types. For ~67 per cent of the event data set our  $M_e$  differs  $\leq \pm 0.3$  magnitude units (m.u.) from the respective  $M_e$  values published by the USGS. However, larger discrepancies (up to 0.8 m.u.) may occur for strike-slip events. A reason of that may be the overcorrection of the energy flux applied by the USGS for this type of earthquakes. We follow the original definition of magnitude scales, which does not apply *a priori* mechanism corrections to measured amplitudes, also since reliable fault-plane solutions are hardly available within 10–15 min after the earthquake origin time. Notable is that our uncorrected  $M_e$  data show a better linear correlation and less scatter with respect to  $M_w$  than  $M_e$  of the USGS. Finally, by analysing the recordings of representative recent pairs of strong and great earthquakes, we emphasize the importance of combining  $M_w$  and  $M_e$  in the rapid characterization of the seismic source. They are related to different aspects of the source and may differ occasionally even more than 1 m.u. This highlights the usefulness and importance of providing these two magnitude estimates together for a better assessment of an earthquake's shaking potential and/or tsunamigenic potential.

**Key words:** Time series analysis; Earthquake source observations; Body-waves.

### INTRODUCTION

In recent years, a number of authors have focused their activity on improving and developing faster procedures to properly calculate the magnitude of an earthquake in a short time after its occurrence

(e.g. Okal & Talandier 1989; Sipkin 1994; Tsuboi *et al.* 1995; Lomax *et al.* 2007; Bormann & Saul 2008, 2009; Kanamori & Rivera 2008; Lomax & Michelini 2009). Many efforts have been initiated after the great 2004 December 26 Sumatra earthquake, when the limitations of the standard procedures adopted at that time

by many agencies failed to provide accurate magnitude estimates of this event in time to launch early enough warnings and appropriate response. Indeed, since then, much progress has been made, even though rapid earthquake magnitude determination procedures may yield values that differ by a few tenths of magnitude units (m.u.) from final values because of less accurate input values, for example, of automatic hypocentre locations.

A prompt and reasonably accurate initial estimate of an earthquake's damage potential is of great importance for improved guidance of the rapid response activities of disaster management organizations. This is particularly the case when earthquakes occur in areas that are not well monitored by near- or real-time local networks. Then estimates of the fundamental parameters hypocentre location and earthquake magnitude may have to be based on teleseismic data only. Since no single magnitude determination can sufficiently describe the static and dynamic aspects of earthquake ruptures as well as their complexity in space and time, different complementary magnitude determinations should be used together (e.g. Kanamori 1983; Bormann *et al.* 2002) for a better characterization of the seismic sources. However, nowadays it is common practice to use for this purpose only the moment magnitude  $M_w$ . Being based on the seismic moment  $M_0$ , which is related to the low frequency asymptote of the far field displacement spectrum,  $M_w$  is a good measure of the 'earthquake's size' in terms of the product of fault area times average displacement and thus fundamental for evaluating the tsunami potential. However,  $M_w$  does not provide information about the complexity and dynamics of the rupture and thus the related high frequency content radiated by the seismic source (e.g. Beresnev 2009). In contrast, the energy magnitude  $M_e$ , based on the radiated seismic energy  $E_s$ , is more suitable than  $M_w$  for evaluating the earthquake's shaking potential (Choy & Boatwright 1995; Choy & Kirby 2004) since  $E_s$  is proportional to the squared ground motion velocity and is calculated over a wide frequency range that is much closer to frequencies of engineering interest. Therefore,  $M_e$  is a useful complement to  $M_w$  in the rapid evaluation of the damage potential of large earthquakes.

Among the many procedures developed to rapidly provide sufficiently accurate magnitude estimates, one to determine also the energy magnitude  $M_e$  is needed. Recently, Di Giacomo *et al.* (2008) developed a procedure to calculate  $M_e$  soon after the earthquake's origin time (OT), which is suitable for implementation in rapid response systems. The procedure proved to be promising by calculating  $M_e$  for the great 2004 December 26 Sumatra earthquake within 15 min without requiring any modification of the procedure, despite the exceptional nature of this event. In this paper, we outline the modifications of the approach by Di Giacomo *et al.* (2008) and verify its applicability. To do this, we analysed the broad-band teleseismic recordings relevant to 767 earthquakes globally distributed. An empirical validation of the synthetic spectral amplitude decay functions used for correcting the observed spectra is also shown. Then, to assess the suitability of our approach, we compare our rapid  $M_e$  with the  $M_e$  and  $M_w$  provided by the NEIC/USGS (<http://neic.usgs.gov/neis/sopar/>) and the  $M_w$  by the GCMT ([www.globalcmt.org](http://www.globalcmt.org)). Finally, the importance of comparing  $M_w$  and  $M_e$  is illustrated by considering representative pairs of earthquakes with similar locations and  $M_w$ , but with different  $M_e$ .

## ANALYSED DATA SET

The data set considered in this work includes 767 worldwide distributed shallow earthquakes ( $h < 70$  km) in the magnitude range

$5.5 \leq M_w \leq 9.0$ . They occurred between 1990 March and 2007 December. In addition, the  $M_w$  7.9 Wenchuan earthquake of 2008 May 12 has been included. Table A1 in the supplementary material lists the source parameters for the analysed events. For each earthquake, we analysed the vertical component of the broad-band recordings provided by permanent stations belonging to either a global (IRIS/IDA, IRIS/USGS, GEOFON and GEOSCOPE) or a regional network. Of course, the number of stations available and used in the analysis is much larger both for large earthquakes and for those that occurred over the last few years, as the global networks have been expanded. Here we are interested only in shallow earthquakes, which are the most important ones in terms of damage potential. After removing stations with poor signal-to-noise ratio, we obtained in total about 40 000 single stations  $M_e$  determinations. Given the size of the data set considered, also for each earthquake magnitude estimation, the different source–receiver propagation paths sample a large volume of the Earth's medium. Since we use an average 1-D earth model (as explained in the following), this allows us to average out the scatter of individual observations due to heterogeneities along the path, as demonstrated by two examples in the next section.

We grouped the analysed earthquakes according to their GCMT fault plane solutions using the classification given by Zoback (1992). Fig. 1 shows their geographical distribution. Table 1 lists the number of earthquakes for each class of source geometry. The data set is strongly dominated by thrust and strike-slip earthquakes. Although we do not apply specific corrections for the different radiation patterns, such a classification will be useful when discussing our results and for better understanding the influence of source mechanisms on the calculated energies.

## RAPID DETERMINATION OF $M_e$ (GFZ)

This section recalls some of the theoretical basics and assumptions underlying the calculation of the radiated seismic energy in the teleseismic range by using  $P$ -waves waveforms (for more details, the reader is referred to, for example, Haskell 1964; Rudnicki & Freund 1981; Vassiliou & Kanamori 1982; Boatwright & Fletcher 1984; Boatwright & Choy 1986; Venkataraman & Kanamori 2004a,b). Further, we outline the modifications made to the procedure described in Di Giacomo *et al.* (2008).

The energy radiated as seismic waves by the seismic source can be obtained by integration with frequency of the squared spectrum of the derivative of the moment tensor rate  $\hat{M}(f)$

$$E_s = \left[ \frac{1}{15\pi\rho\alpha^5} + \frac{1}{10\pi\rho\beta^5} \right] \int_{f_1}^{f_2} |\hat{M}(f)|^2 df, \quad (1)$$

where  $\alpha$ ,  $\beta$  and  $\rho$  represent the  $P$ -wave velocity, the  $S$ -wave velocity and the density at the seismic source, respectively,  $f$  is the frequency and  $f_1$  and  $f_2$  are the lower and upper bounds of the integration, respectively.

In this equation, the source spectrum is obtained by considering teleseismic  $P$  waves under the point source assumption. The use of  $P$  waves has some advantage with respect to  $S$ -waves: (1) they are the faster waves and therefore arrive first at the seismic stations. This is essential for rapid earthquake magnitude determinations and (2) they are less affected than  $S$  waves by energy loss during wave propagation.

The right-hand side of eq. (1) can be described by considering the term in squared brackets outside the integral (hereinafter called  $k$ ) and the integral itself. The term  $k$  [having the unit of  $s^3$  (Nm) $^{-1}$ ]

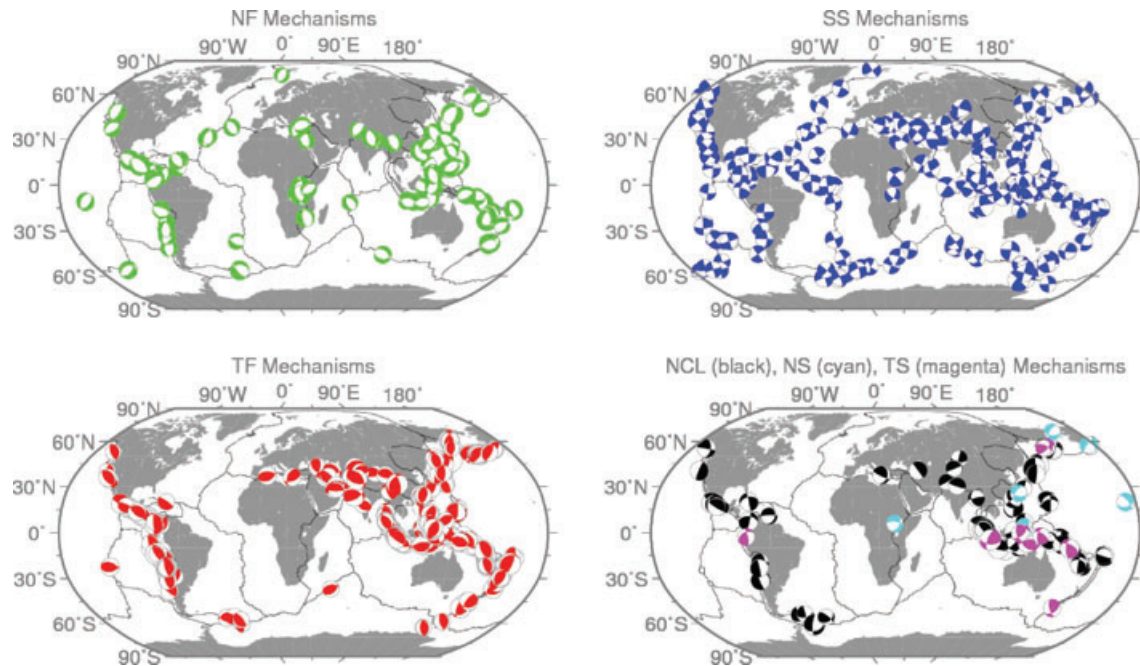


**Figure 1.** Maps showing the distribution of the earthquakes and their types according to the classification of Zoback (1992). Normal faulting (NF) solutions are plotted in green, strike-slip (SS) solutions in blue, thrust (TF) solutions in red, not classified (NCL) solutions in black, normal with strike-slip component (NS) solutions in cyan, and thrust with strike-slip component (TS) solutions in magenta. The plate tectonic boundaries have been plotted according to Bird (2003).

**Table 1.** Summary of the grouping of the focal solutions for the analysed data set using the classification of Zoback (1992).

Focal mechanism type	Thrust (TF)	Strike-slip (SS)	Normal (NF)	Not classified (NCL)	Thrust with strike-slip component (TS)	Normal with strike-slip component (NS)
Number of earthquakes	315	260	99	74	11	8

depends on the properties of the medium surrounding the source volume and could also be rewritten in terms of the  $S$ - to  $P$ -wave energy ratio  $q = 1.5(\alpha/\beta)^5$  (which holds under the point source condition), and replacing  $\alpha$  or  $\beta$  accordingly. The Earth (and especially the Earth's crust) is a heterogeneous medium, both vertically and laterally. Accordingly,  $k$  may vary over local and regional scales and with depth. This may be a source of uncertainty in the energy estimation. Being interested in calculating  $M_e$  in a rapid way for global earthquakes with source depths  $< 70$  km, we only account for vertical heterogeneities by using the average global 1-D reference earth model AK135Q (Kennett *et al.* 1995; Montagner & Kennett 1996). For sake of practicality, we separate the earthquakes into two groups with source depth shallower or deeper than 18 km, and use the respective values of  $\alpha$ ,  $\beta$  and  $\rho$  given for the 1-D spherical average structure of the model AK135Q, that is, for events shallower than 18 km depth  $\alpha = 6.8 \text{ km s}^{-1}$ ,  $\beta = 3.9 \text{ km s}^{-1}$  and  $\rho = 2.92 \text{ g cm}^{-3}$  and for the deeper ones  $\alpha = 8.0355 \text{ km s}^{-1}$ ,  $\beta = 4.4839 \text{ km s}^{-1}$  and  $\rho = 3.641 \text{ g cm}^{-3}$ , respectively. The 18 km boundary has been chosen because changes in depth above and below it do not introduce very large discrepancies in the  $M_e$  estimates. With regard to this, in Di Giacomo *et al.* (2008), different values of  $\alpha$ ,  $\beta$  and  $\rho$  were used for very shallow events ( $h \leq 10$  km) which caused, together with the long  $S$ - $P$  time windows, an overestimation (up to 0.6 m.u.) for some events with respect to the  $M_e$  values reported here. With the modification now made, even in the worst case scenario of a wrong hypocentre depth calculation by the near- or real-time location procedure, the use of the corresponding depth values of  $\alpha$ ,  $\beta$  and  $\rho$  in eq. (1) for either  $h < 18$  km or  $18 \text{ km} \leq$

$h < 70$  km would result in  $M_e$  values that are biased by not more than  $\pm 0.25$  m.u., which is still acceptable for rapid response purposes.

In theory, the integral term of (1) should be calculated over the whole frequency band spanned by the source spectrum. However, in practice there are frequency band limitations, in particular towards higher frequencies of the exploitable source spectrum. As a rule, the low frequency limit  $f_1$  should be selected according to the length of the  $P$ -wave time window  $t_p$  considered in the analysis for the energy calculation and be not lower than  $f_1 = 1/t_p$ . The length of the time window should include the whole duration of the earthquake rupture (i.e. the time when the source is dynamically rupturing) so as to avoid time window saturation effects (e.g. Bormann *et al.* 2007). Here, the duration time is estimated using the technique of Bormann & Saul (2008, 2009), which is similar to the one of Lomax *et al.* (2007). The duration obtained by this technique is a rough estimate (generally larger) of the actual rupture duration and is meant to guarantee that the signal relevant to the radiated energy calculation is included in the time window. Thus,  $PP$  and  $PPP$  phase arrivals at later times are not included in the single station  $M_e$  determinations for the large majority of the data set. The effect of using the complete  $S$ - $P$  time windows has been discussed in Di Giacomo *et al.* (2008). In particular, the use of such long time windows will include later phases (like  $PP$  and  $PPP$ ), which may cause an overestimation of  $M_e$  that should not be larger than 0.2 m.u. (see also Choy & Boatwright 2007). On the other hand, the high frequency limit of the integration  $f_2$  is mostly determined by the poor SNR, especially for frequencies  $> 1$  Hz at teleseismic distances. This represents a severe limitation in

the possibility of calculating  $M_e$  in the teleseismic range for events smaller than  $\sim 5.5$ , which require, because of their short rupture duration, higher frequencies to be recorded and analysed.

In this study, the integration limits are  $f_1 \sim 12$  mHz and  $f_2 = 1$  Hz. The limitation at 1 Hz is also determined by the fact that the Q structure in the model AK135Q has been obtained from data with minimum period of 1 s (Montagner & Kennett 1996). Therefore, using this model for calculating Green's functions at higher frequencies would not be appropriate. Despite these bandwidth limitations, since the corner frequencies for moderate to great earthquakes usually lay within the used frequency band and the radiated seismic energy is proportional to the square of the velocity, the part of the source spectrum that is not considered in the calculation ( $f < f_1$  and  $f > f_2$ ) will not significantly affect our  $M_e$  estimations (in the worst case scenario of  $\sim 0.2$  m.u.). Different authors adopt different low and high frequency limits  $f_1$  and  $f_2$ . For example, Choy & Boatwright (1995) use frequencies between 10 mHz and 5 Hz as the maximum bandwidth, whereas Newmann & Okal (1998) use 14 mHz as  $f_1$  and 2 Hz as  $f_2$ , while others (e.g. Polet & Thio 2003; Venkataraman & Kanamori 2004b) also use  $f_2 = 1$  Hz for calculating source spectra and the related radiated energies for significant earthquakes. Of course, the chosen limits are tuned also to the investigated magnitude range.

In order to obtain an estimation of  $|\hat{M}(f)|$  at a single station, we must account for the frequency dependent  $P$ -wave's energy losses due to geometrical spreading and anelastic absorption, which occur during the paths from the source to the receivers through the layered structure of the Earth. This is one of the most problematic aspects of calculating the energy. Correction of the wave propagation effects and the related frequency-dependent energy loss would require a detailed knowledge of the Earth's heterogeneous struc-

ture. One powerful tool used to describe and account for the effect of the Earth medium consists of numerical simulations of Green's functions.

Adopting the already mentioned model AK135Q, we use a self-developed code QSSP to calculate the synthetic seismograms for the spherical earth model. The new code is based on the propagator algorithm proposed by Gilbert & Backus (1968) but extended with the orthonormalization technique (Wang 1999) to ensure the numerical stability. In general, QSSP provides more reliable Green's functions than the reflectivity code particularly in the low frequency range and thus allows us to extend the lower bound  $f_1$  of the frequency band considered in our calculations from 16.6 mHz (Di Giacomo *et al.* 2008) to 12.4 mHz. As already described and shown in Fig. 1 of Di Giacomo *et al.* (2008), the synthetic  $P$ -waves spectral amplitude decay functions in the distance range  $20^\circ$ – $98^\circ$  have been calculated for 20 different frequencies. Since our method is designed to work without prior knowledge of the fault plane and slip geometry, we use the median values of these functions and compute an estimation of  $|\hat{M}(f)|$  at the single station simply from the ratio, for each selected frequency, between the observed velocity spectral amplitude  $\hat{u}(f)$  and the corresponding value of the spectral amplitude decay function at a given frequency  $f$  and distance  $\Delta$ . As the spectral amplitude decay functions are available in tabulated form, the calculation of the radiated energy can be performed in a very rapid way. Fig. 2 shows observed velocity spectral amplitudes versus distance for two frequencies (periods), 1 Hz (1 s) and 0.0625 Hz (16 s) for two recent earthquakes. Fig. 2(a) refers to the Mw 6.9 north of the Molucca Sea earthquake of 2007 July 26 (event #701 in Table A1) and Fig. 2(b) relates to the Mw = 7.9 Wenchuan earthquake of 2008 May 12 (#767 in Table A1). The spectral amplitude decay functions (calculated by using the simulation code of QSSP) for the same

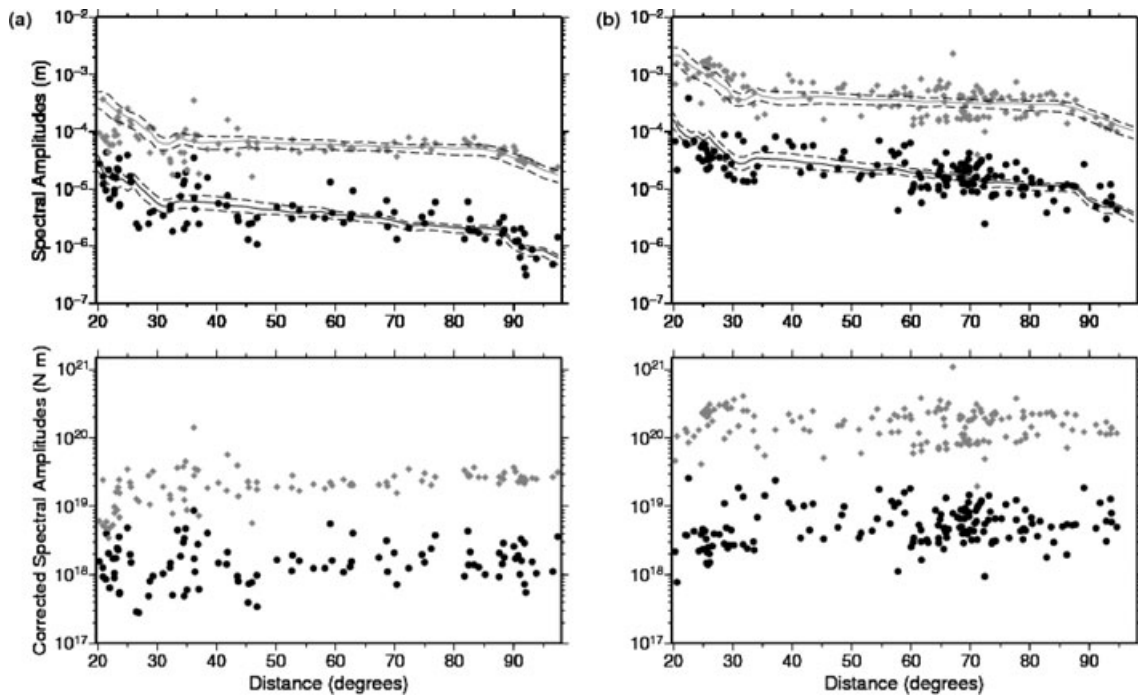


**Figure 2.** (a) The upper panel shows the observed velocity spectral amplitudes with distance from the source for frequencies of 1 Hz (black circles) and 0.0625 Hz (grey circles) for event #701 in Table A1; the median of the spectral amplitude decay functions (which have units of  $\text{m s/N m}$ ) at 1 and 0.0625 Hz (solid black line and grey lines, respectively) are shown together with their corresponding 15th and 75th percentiles and have been shifted by an arbitrary offset in order to make easier the comparison with the real data. The lower panel shows the corresponding displacement spectral values after applying the correction at each station and scaling them to seismic moment. (b) The same as for Fig. 2a, but for event #767 in Table A1.

frequencies have been plotted by adding an arbitrary offset in order to ease the comparison of the observed data with the simulations. After applying the correction, one can expect that the corrected spectral amplitude values are on average independent of distance.

Fig. 2 shows that, although individual measured data points may scatter significantly around the medians of the synthetic functions due to heterogeneities in the real Earth, the simulations are able to reproduce the average trend of the observations. In fact, the deviation of the actual Earth structure from its 1-D average for specific source–receiver paths (which may influence different frequencies in different ways), and/or the effects of the fine 3-D velocity and  $Q$  structure just below the seismic stations, the seismic source finiteness, directivity and radiation pattern, all may contribute to a different extent to the variability of the single station  $M_e$  estimates. Therefore, stable event magnitude estimates necessitate to analyse and average as many observations as possible in order to minimize the influence of this data scatter, which is about the same in all distance ranges between  $20^\circ$  and  $98^\circ$  (Fig. 3). For our rapid procedure, we require at least three station estimates of  $M_e$  before computing the first arithmetic event average. When more than 8 station estimates become available, we take as the final  $M_e$  value the 25 per cent truncated mean (e.g. Bormann & Saul 2008). The latter is advisable especially in an automatic procedure since it excludes outliers that may deviate significantly from the average.

The distribution of all  $M_e$  station residuals over epicentral distance is shown in Fig. 3. Including stations at distances between  $20^\circ$  and  $30^\circ$  allows us to launch the procedure (and to provide eventually alarm  $M_e$ 's) earlier. According to Fig. 3, data collected within this upper mantle  $P$ -wave triPLICATION range do not scatter more than those at larger teleseismic distances and thus do not adversely bias the final  $M_e$  event averages. The median residual values for bins  $10^\circ$  wide and  $5^\circ$  overlap were all within only  $\pm 0.064$  m.u., with negative values up to  $\sim 60^\circ$  and positive ones at larger distances. The uneven distribution of the global station's deployment (concentrated in Europe and North America) and of the source–receiver paths may contribute to such a residual pattern.

Fig. 4 shows an example of the  $M_e(\text{GFZ})$  residuals for two recent great earthquakes (which will also be considered later in the paper). They occurred recently in the Kuril Islands arc, have been

recorded by many broad-band stations, and differ in their location by only about 100 km. Thus, the propagation paths to stations in the teleseismic range are about the same for both events. We note a very similar distribution of the residuals for these two events despite their different source mechanism. This hints to a dominating influence of the real Earth heterogeneities with respect to the model and emphasizes the importance of using globally distributed stations in order to minimize their effect on event  $M_e$  estimates.

Next, we compare our rapid  $M_e$  determinations for the 767 events analysed with the moment magnitude  $M_w$  and  $M_e$  from NEIC/USGS.

## COMPARISONS OF $M_w$ AND $M_e$

For large earthquakes,  $M_w$  from the Global Centroid Moment Tensor project ([www.globalcmt.org](http://www.globalcmt.org)) is commonly used as the reference for any other magnitude.  $M_w(\text{GCMT})$  is obtained from the inversion of very long-period waveforms of  $S$  and surface waves, which are necessary to get an accurate determination of the seismic moment  $M_0$ . However, the drawback of analysing very long periods is that  $M_w(\text{GCMT})$  is usually not available within less than one hour after OT. In contrast,  $M_w$  estimations of the NEIC/USGS (Sipkin 1994), based e.g. on broad-band  $P$ -wave records, are provided much sooner and are used by many agencies (e.g. WAPMERR, <http://www.wapmerr.org/>) to rapidly evaluate the earthquake's impact. According to our data set,  $M_w(\text{USGS})$  and  $M_w(\text{GCMT})$  differ by only  $\pm 0.2$  m.u. for about the 90 per cent of the data, with the tendency, however, of  $M_w(\text{GCMT})$  to be generally larger than  $M_w(\text{USGS})$ , especially for  $M_w > 8$ .

In Fig. 5 we compare our rapid  $M_e$  determinations with the  $M_w(\text{GCMT})$  and the  $M_w(\text{USGS})$ . For 47 earthquakes  $M_w(\text{USGS})$  is not available in the SOPAR database (<http://neic.usgs.gov/neis/sopar/>).  $M_w(\text{GCMT})$  and  $M_w(\text{USGS})$  are both generally larger than  $M_e(\text{GFZ})$ . On average,  $M_w(\text{GCMT})$  is larger than  $M_e(\text{GFZ})$  by  $\sim 0.19$ ,  $\sim 0.17$  and  $\sim 0.16$  m.u. for the SS, NCL and TF mechanisms, respectively. For the other mechanism groups (NF, NS, and TS) the average difference is smaller than 0.1 m.u.

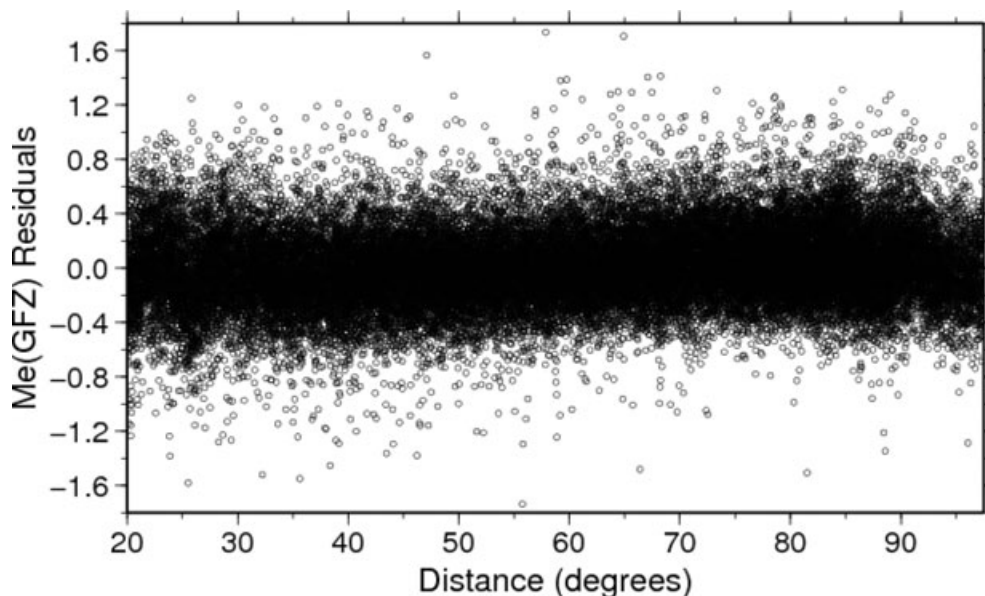


**Figure 3.** Distribution of the  $M_e(\text{GFZ})$  station residuals with distance for the complete data set considered in this work. See text for details.

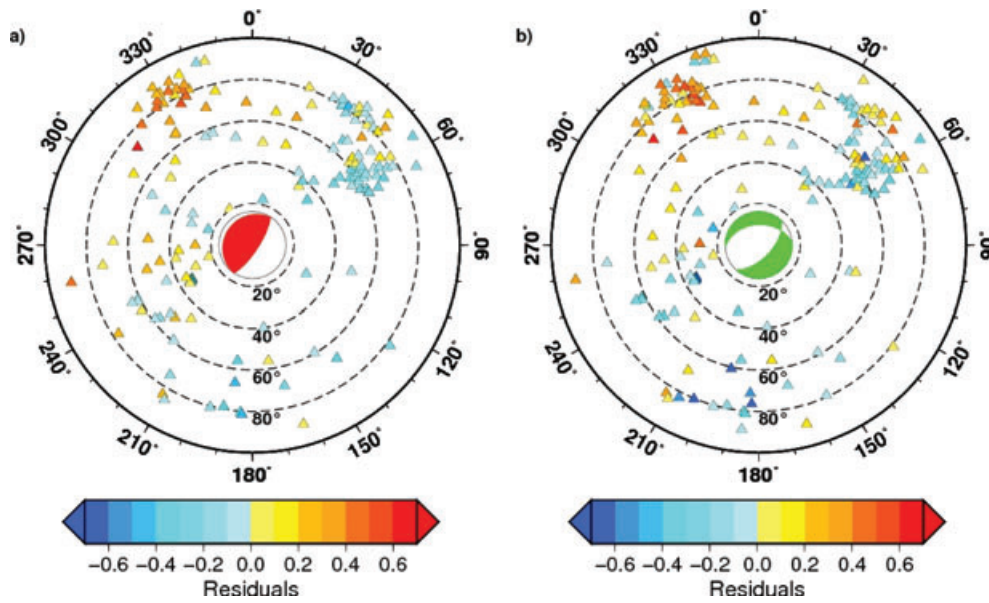


**Figure 4.** Plots in polar projection of the residuals of Me(GFZ) for event #623 (a) and #636 (b) in Table A1. The corresponding fault plane solutions are plotted in the centre of the diagrams. The dashed circles represent the distance from the source in degrees. See text for details.

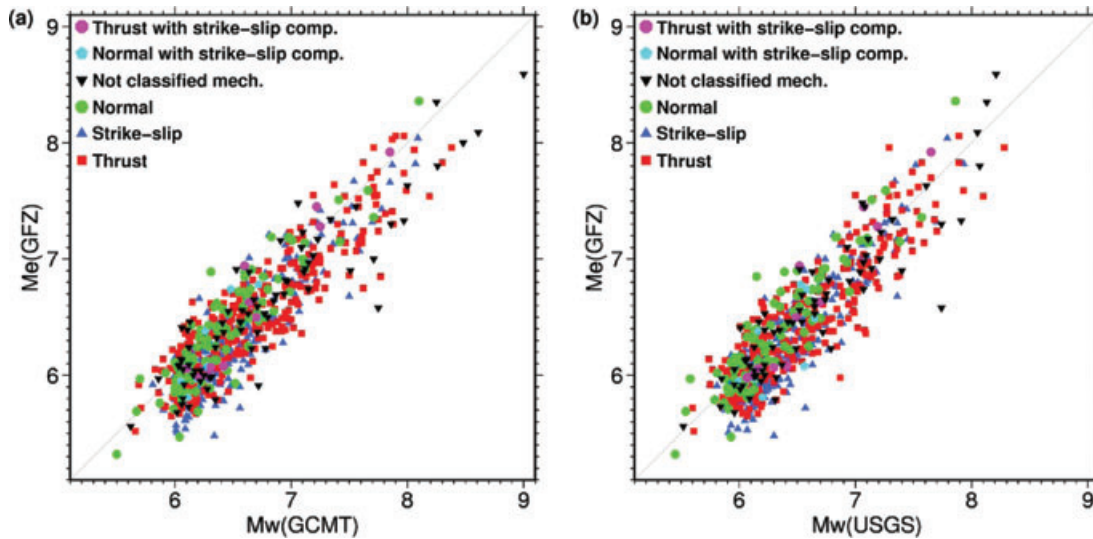


**Figure 5.** Comparison of a) Mw(GCMT) with Me(GFZ) for 767 events, and b) Mw(USGS) with Me(GFZ) for 720 events. Different symbols represent the type of mechanism. The 1:1 lines are also plotted.

Similar findings apply to the comparison Mw(USGS)-Me(GFZ), with a maximum average difference of  $\sim 0.14$  m.u. for SS events. However, in analysing these average differences, we must also consider that in most of the analysed data sets of strong to great earthquakes the number of events characterized by a deficiency in high frequency radiation (e.g. slow earthquakes and/or TF and NCL events in subduction zones with possibly anomalous low stress drop and/or rupture velocity, which is normally translated in a smaller Me), is larger than those of events enriched in the high frequency radiation (possibly characterized by high stress drop and/or rupture velocity, for which a larger Me is expected). However, in the absence of any *a priori* source mechanism-dependent correction applied to our measured  $E_S$  values we do not observe any systematic trend in the differences between Mw and Me(GFZ) due to the

focal mechanism type. This agrees also with Schweitzer & Kväerna (1999), who investigated the influence of source radiation patterns on globally observed short-period magnitude estimates mb. They concluded that the effect of the source radiation pattern on the amplitudes used for mb estimation on a global scale is relatively small compared to effects from other factors and much smaller than theoretically expected on the basis of standard source and earth models. Thus, differences between corrected and uncorrected mb event magnitudes were always within  $\pm 0.15$  m.u.

The NEIC/USGS have calculated Me on a routine basis using the procedure of Boatwright & Choy (1986) since 1987. This procedure requires knowledge of the fault plane solution in order to apply the correction for the radiation pattern. In past years, the following relationship for Me calculation has been used (e.g. Choy *et al.*

2006):

$$M_e = 2/3(\log_{10} E_S) - 2.9. \quad (2)$$

However, as recommended by Bormann *et al.* (2002), we determine  $M_e$  as follows:

$$M_e = 2/3(\log_{10} E_S - 4.4), \text{ with } E_S \text{ given in Joule.} \quad (3)$$

Relationship (3) is now also accepted at the NEIC as standard. To avoid occasional rounding errors of 0.1 m.u. between (2) and (3), we recalculated pre-2008  $M_e$ (USGS) values according to eq. (3) from the  $E_S$  reported in the SOPAR database and rounded them to the nearest hundredth. This way we assure a correct comparison between  $M_e$ (USGS) and  $M_e$ (GFZ).

The comparison between  $M_w$ (GCMT) and  $M_e$ (USGS), as well as  $M_e$ (USGS) and  $M_e$ (GFZ), for 637 earthquakes is shown in Figs 6(a) and (b), respectively. For 130 earthquakes analysed by us, there are no  $M_e$ (USGS) values available in the SOPAR database. The average difference  $M_w$ (GCMT)- $M_e$ (USGS) is  $\sim 0.27$ ,  $\sim 0.21$  and  $\sim 0.18$  m.u. for TF, NCL and NF events, respectively. However, the most important feature of Fig. 6(a) is that  $M_e$ (USGS) for SS earthquakes is generally larger (on average  $\sim 0.26$  m.u.) than  $M_w$ (GCMT), suggesting a significant dependence of  $M_e$ (USGS) on the focal mechanism corrections for SS events. As shown in Fig. 5, this is not the case for the uncorrected  $M_e$ (GFZ) estimates, which scale more linear and with less scatter than  $M_e$ (USGS) with  $M_w$ (GCMT).

For about 67 per cent of the analysed earthquakes, the differences between  $M_e$ (USGS) and  $M_e$ (GFZ) is within  $\pm 0.3$  m.u., which is a satisfactory result for a rapid procedure compared to a more formal one. For  $M_e \leq 6$ ,  $M_e$ (GFZ) is on average 0.2 m.u. larger than  $M_e$ (USGS) and 0.1 m.u. smaller for  $M_e > 6$ . By considering the different source mechanism types for all magnitude range, for dip-slip events (NF and TF events)  $M_e$ (GFZ) is on average  $\sim 0.1$  m.u. larger than  $M_e$ (USGS), whereas for SS events  $M_e$ (USGS) is on average  $\sim 0.4$  m.u. larger than  $M_e$ (GFZ). For all the other mechanism types the average difference between  $M_e$ (USGS) and  $M_e$ (GFZ) is close to zero.

In this context we refer to Newman & Okal (1998), who also modified the method of Boatwright & Choy (1986) to make it suitable for implementation in a real-time procedure for the dis-

crimination of tsunami earthquakes by means of the parameter  $\Theta = \log_{10} E_S / M_0$ . Analysing a data set of 52 earthquakes, they found that their  $E_S$  values for the 5 strike-slip events included in their data set were much smaller than the ones from NEIC/USGS (up to 1.4 order of magnitude), and also that their  $E_S$  values were generally larger for all the other types of earthquakes. The large discrepancies for the strike-slip events were attributed by Newman & Okal (1998) to the overcorrection of the energy flux by the USGS when using, according to theory, small values for the radiation pattern correction, whereas the heterogeneities of the real Earth allow the high frequency content to find its way into the seismograms along non-geometrical paths. This is in agreement with the findings and interpretation of mechanism-dependent mb corrections by Schweitzer & Kväerna (1999).

More recently, Pérez-Campos & Beroza (2001) extended the method of Boatwright & Choy (1986) in order to include the uncertainties in the factors involved in the  $E_S$  determination (e.g. focal mechanism, attenuation, spectral fall off, etc.). They analysed 204 earthquakes (58 strike-slip, 101 thrust and 45 normal-faulting earthquakes) and found their  $E_S$  estimates to be generally smaller than the NEIC/USGS estimates for all mechanism types, but with the strike-slip earthquakes showing the largest differences. However, Pérez-Campos & Beroza (2001) confirmed the persistence of a larger apparent stress drop for the strike-slip earthquakes with respect to the other type of events, which may result in slightly larger  $M_e$  values for such events.

Other reasons than source mechanism-corrections for such discrepancies may be differences in the methodologies when correcting the spectra for attenuation. Although the aim of this work is not a detailed investigation of the influence of the focal mechanism on the energy estimates (which would be the subject of a different study), the consistency of our results also with some previous studies confirm that our procedure is a suitable contribution to the assessment of the earthquake's damage potential by providing rapid energy magnitude estimates, which have been obtained, according to the original magnitude concept, without specific source radiation pattern corrections.

However, regardless of the discrepancies between  $M_e$ (USGS) and  $M_e$ (GFZ), especially for the strike-slip earthquakes, Figs 5 and 6(a) show that  $M_w$  and  $M_e$  can be significantly different, as already

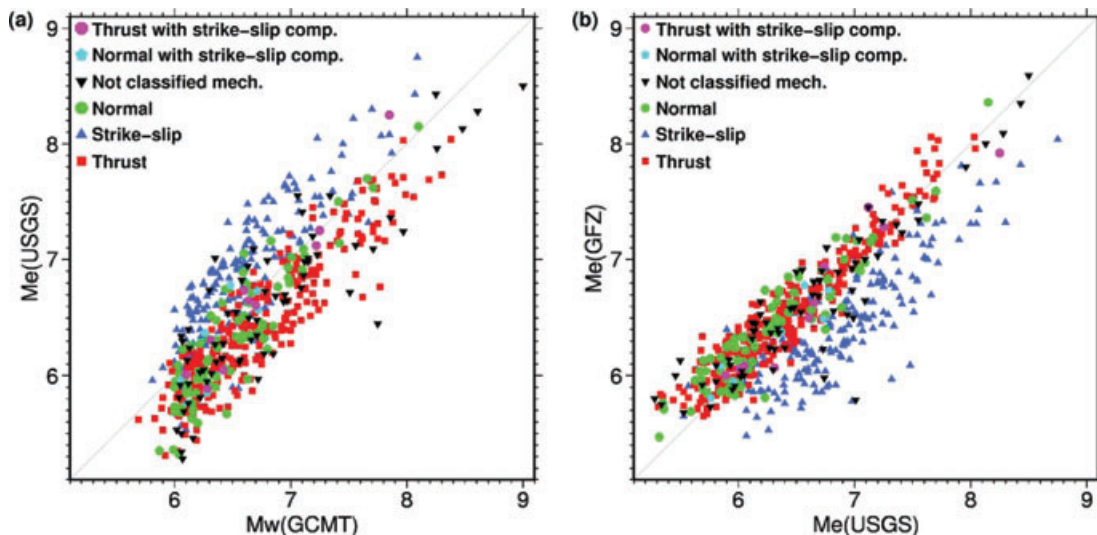


**Figure 6.** Comparison of (a)  $M_w$ (GCMT) with  $M_e$ (USGS) and (b)  $M_e$ (USGS) with  $M_e$ (GFZ) for a total of 637 earthquakes. Different symbols represent the type of mechanism. The 1:1 lines are also plotted.

highlighted by several authors (e.g. Purcaru & Berckhemer 1978; Choy & Kirby 2004). It is also important to remind the reader that  $M_w$  was derived under the assumption of constant stress drop  $\Delta\sigma$  (Kanamori 1977; Hanks & Kanamori 1979) and thus a constant ratio  $E_S/M_0 = \Delta\sigma/2\mu$  (with  $\mu =$  rigidity), although observations indicate that this ratio spreads over at least three orders of magnitude (e.g. Choy & Boatwright 1995; Weinstein & Okal 2005; Lomax & Michelini 2009). Therefore, as  $M_w$  provides information about the static and  $M_e$  about the dynamic properties of the seismic source, respectively, they should be used jointly for a better assessment both of the tsunami and shaking potential of large earthquakes soon after their occurrence. This point is emphasized by the following representative examples.

## REPRESENTATIVE CASE STUDIES

In this section, we consider for different seismotectonic regions pairs of earthquakes with a similar location within the considered area. For each pair, the analysis results at one of the recording stations are shown, in order to illustrate the importance of characterizing an earthquake by both its  $M_w$  and  $M_e$ .

### The 2006 November 15 and the 2007 January 13 Kuril islands earthquakes

These two recent great earthquakes represent an extraordinary example since they occurred very close in space and time and show a significant difference in the observed short-period body wave amplitudes despite of their similarity in seismic moment (Ammon *et al.* 2008).  $M_w$ (GCMT) is equal to 8.3 for the 2006 November 15 event and 8.1 for the 2007 January 13 event, but the high frequency part of the energy release of the latter was higher. This is confirmed by the different  $M_e$  values for the 2006 and 2007 earthquake:  $M_e$ (GFZ) 7.83 and 8.36, and  $M_e$ (USGS) 7.73 and 8.15, respectively. For both earthquakes, a large number of seismic stations has been used to compute  $M_e$ (GFZ), and 82 of them are in common (see Fig. 7), so that the redundancy of the information provided by the observations is very high in both cases. Hence, since the locations of these two earthquakes differ by only about 100 km, the paths from the source to receivers at teleseismic distances are practically the same. Therefore, it is reasonable to assume that differences in the observed short periods body wave amplitudes are mainly due to different source characteristics. In Fig. 8, from the top to the bottom panels, the  $S$ - $P$  windows and their high frequency  $P$ -wave envelopes (Bormann & Saul 2008), the time-frequency analyses via the  $S$ -transforms (Stockwell *et al.* 1996; Parolai 2009) of the windows used to include the rupture duration, as well as the  $E_S$  (left-hand  $y$ -axis) and  $M_e$  values (right-hand  $y$ -axis) for cumulative  $P$ -wave windows for the station INCN are shown. All results underline the different high-frequency radiation content of these two earthquakes. The time-frequency analysis performed with the  $S$ -transform allows us to better highlight and describe the information provided by the seismic recordings before applying any correction to the data. The  $S$ -transform amplitudes for the different frequencies show significant differences for these two events. The 2007 January 13 earthquake (right-hand panels in Fig. 8) radiated a large amount of energy at  $\sim 0.1$  Hz just after the  $P$ -wave arrival (first 15–20 s) and important contributions to the total energy release come also from successive arrivals with higher dominant frequencies between 0.2 and 0.4 Hz. In contrast, the 2006 November 15 earthquake (left-hand panels in Fig. 8) radiated seismic energy mainly at lower frequencies ( $\sim 0.1$  and  $\sim 0.03$  Hz), which is spread over a longer

time span. Furthermore, in agreement with its larger seismic moment, the low frequency content around 0.03 Hz is larger than for the 2007 event, whereas the high-frequency content for  $f > 0.1$  Hz is much smaller for the 2006 than for the 2007 earthquake. The same is observed on other station records that have been used in common for both events. This highlights that  $M_w$  alone can not identify and quantify differences in source complexity and energy radiation and calls, therefore, for the need of determining and considering  $M_w$  and  $M_e$  together. These findings confirm the results of Ammon *et al.* (2008), who determined larger moment rate amplitudes in the medium frequency band up to 1 Hz for the 2007 earthquake than for the 2006 event, despite the larger seismic moment of the latter.

Localities in Japan and Russia, which have been affected by this pair of earthquakes, were at about the same distance from the respective epicentres. But according to the NEIC felt reports about these two earthquakes (<http://earthquake.usgs.gov/regional/world/historical.php>), the 2006 earthquake was only slightly felt at some places in Russia and Japan, whereas the shaking due to the 2007 earthquake was much more severe with a maximum intensity of VI observed in several Russian localities. In contrast, the event with the lower shaking intensity generated a tsunami with a maximum measured tsunami wave height of 176 cm, whereas a much smaller tsunami was generated by the 2007 earthquake (maximum measured tsunami wave height 37 cm). Such differences in ground shaking and tsunami generation can be easily explained by the different ratios  $E_S/M_0$  for these two earthquakes. It spans approximately between 2 and  $6 \times 10^{-5}$  for the 2007 earthquake according to our and USGS estimates of  $E_S$ , and thus it is about 10 times larger than for the 2006 event. This is fully reflected in the respective differences  $M_w$ - $M_e$ , which are about +0.2 and  $-0.5$  m.u., respectively.

In order to clarify the amount of time needed by our procedure to provide a stable  $M_e$  in a real- or near-real time implementation, Fig. 7 also shows the  $M_e$  determinations at different times after OT (Fig. 7, bottom panels). Although these two recent great earthquakes occurred in a remote area, our procedure would be able to provide a reliable  $M_e$  already 9–10 min after OT by using less than 20 stations. This still preliminary (alarm)  $M_e$ (GFZ) is already within 0.1 m.u. of the final value obtained by using all available stations. Of course, the time performance of our approach depends on the station availability with respect to the earthquake location. However, the worldwide station deployment is becoming increasingly dense, especially in areas for which a lack of instrumentation was still common a few years ago. Therefore, we are confident that our procedure will yield in the near future rapid  $M_e$  estimates within 10 min after OT also for great earthquakes. In the case of exceptional events with rupture durations of several minutes, such as the great 2004 December 26 Sumatra earthquake, up to 15 min may be needed to obtain a stable  $M_e$  (Di Giacomo *et al.* 2008).

### The 22 April 1991 and the 2 September 1992 Central America earthquakes

Now we present the results for two significant events that occurred on 22 April 1991 and 2 September 1992 in Central America. They are better known as the Costa Rica earthquake and the Nicaragua earthquake, respectively (see Fig. 9). The distance between the two earthquake epicentres is about 500 km, and their seismic moments  $M_0$  are nearly identical, with  $M_w$ (GCMT) = 7.6 for both earthquakes. As these events occurred in the early 1990s, not many broad-band recordings are available of that time. Moreover, the SNR was not sufficient for half of the stations that recorded the Nicaragua

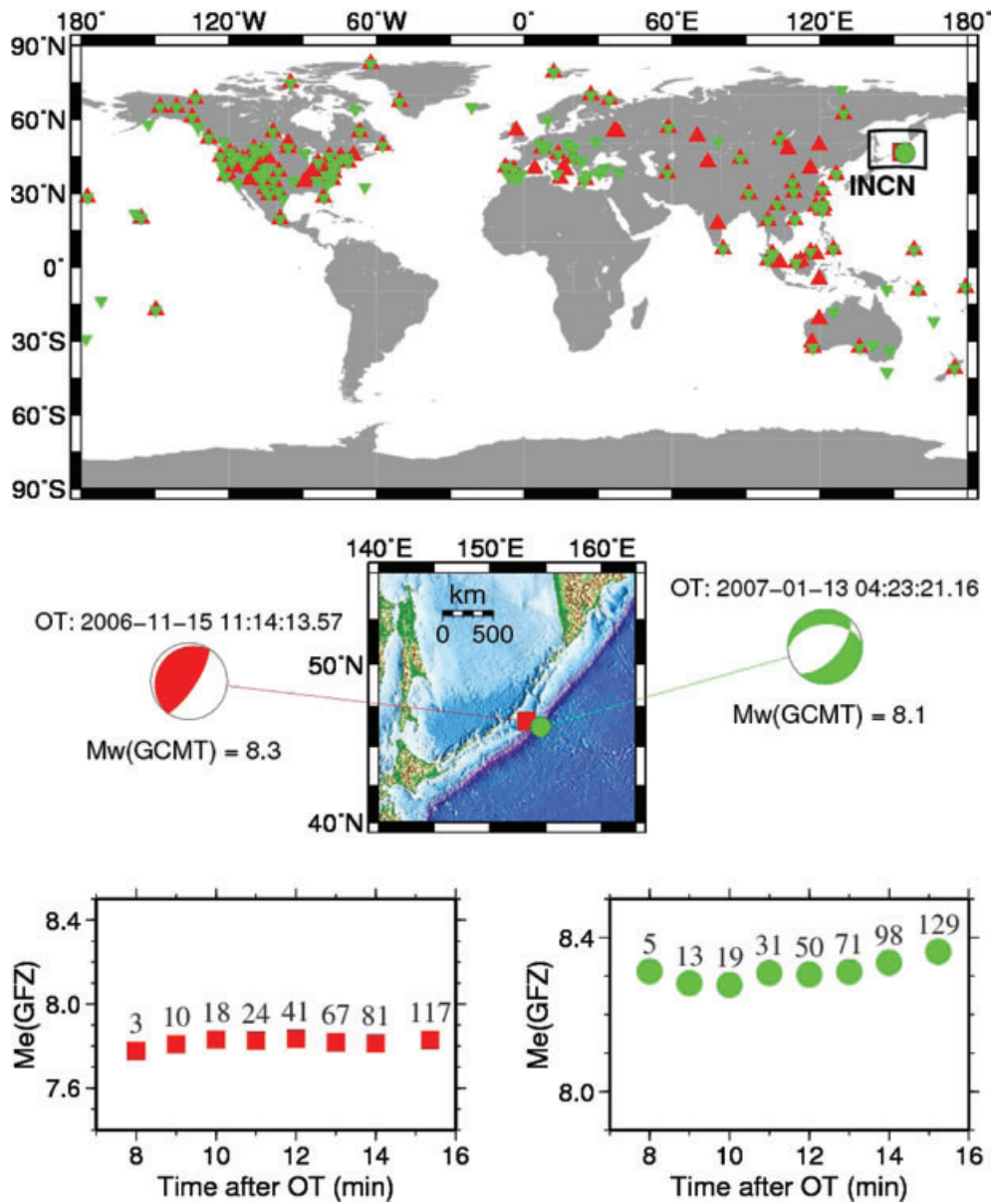


**Figure 7.** Map showing the location of the two Kuril islands earthquakes and the stations used to calculate the final  $M_e(\text{GFZ})$ . The red triangles represent the stations used for the earthquake of 2006 November 15, and the inverted green triangles for the event of 2007 January 13. The station INCEN will be considered in the comparison of Fig. 8. The box delimitates the area shown enlarged in the middle together with the GCMT fault plane solutions and related  $M_w$ . In the lower diagrams  $M_e(\text{GFZ})$  values at different times after OT have been plotted for the 2006 November 15 (left-hand panel) and the 2007 January 13 event (right-hand panel), respectively. The number above each symbol represents the number of stations used at different times after OT.

earthquake. Nevertheless, three seismic stations that recorded both earthquakes have been used (see Fig. 9). In Fig. 10 we show, similarly to Fig. 8, the  $S-P$  windows, the  $S$ -transforms, as well as the  $E_S$  and  $M_e$  values at the station CCM for both earthquakes. Despite nearly identical travel paths of only about 10 per cent difference in length to station CCM, the records of both earthquakes differ strikingly in their more short-period frequency content. The time-frequency analysis reveals that for the Costa Rica event the major contributions to seismic energy come from two distinct energy pulses peaked around  $\sim 0.1$  Hz and  $0.04-0.05$  Hz, respectively, which are a few seconds apart from each other. These two pulses may be associated with the two main rupture patches identified by Goes *et al.* (1993), with the first being smaller and the second being larger. However, according to the  $S$ -transform plot, important burst-

like contributions to the energy release come also from frequencies higher than 0.1 Hz. Thus, the Costa Rica example illustrates the usefulness of the time-frequency analysis in quantifying important details about the source process, which would not be as obvious from the time-domain analysis alone. The Nicaragua earthquake is probably one of the best examples of a slow earthquake generating a large tsunami (e.g. Kanamori & Kikuchi 1993). The energy radiated by this earthquake was significantly depleted in its high frequency content. Indeed, the energy contributions come mainly from below 0.1 Hz and are spread over a longer rupture duration as compared to the Costa Rica event. Yet, the low-frequency  $S$ -transform amplitudes are comparable for both events, as one would expect from their identical  $M_w$ . However, their differences in the observed high-frequency amplitudes are translated into significantly different

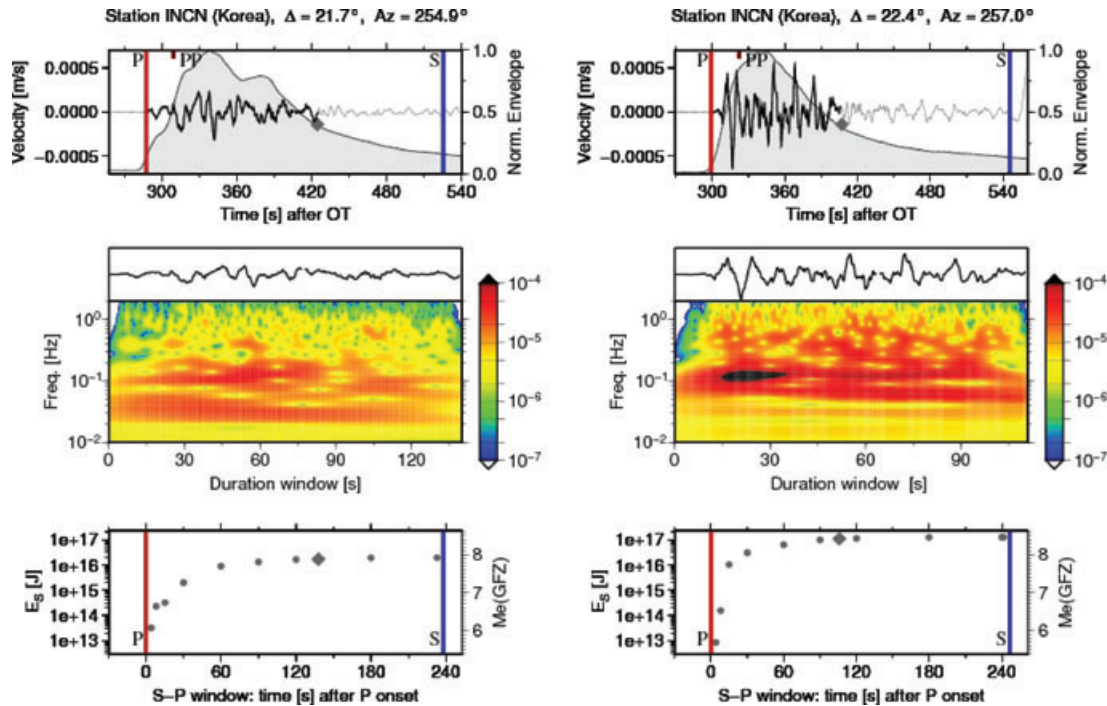


**Figure 8.** The panels on the left-hand side refer to the Kuril islands earthquake of 2006 November 15, and the panels on the right-hand side to the close-by earthquake of 2007 January 13. Upper panels:  $S$ – $P$  time windows of the vertical component velocity seismograms recorded at the station INCN (Korea), with the duration windows marked by the black record trace. Also plotted are the theoretical arrival times of the  $P$ ,  $PP$  and  $S$  phases; the grey shaded area represents the envelope of high-frequency velocity amplitudes used to constrain the overall rupture time duration (Bormann & Saul 2008), and the diamonds at the end of the black record trace mark the end of the time window after the  $P$ -wave onset for which the final  $M_e$ (GFZ) single station value is calculated. Thus, we assure that the full rupture duration is included in the energy calculation. If, however, the rupture duration lasts for several minutes (as for the great 2004 December 26 Sumatra earthquake), the entire  $S$ – $P$  window should be considered. Middle panels: time-frequency analysis via the  $S$ -transform (Stockwell *et al.* 1996; Parolai 2009) calculated over the  $P$ -wave duration window (black record traces in the upper panels that are also shown enlarged just above each middle panel); the colour scales represent the amplitude of the  $S$ -transform in  $\text{m s}^{-1}$  (see text for details). Lower panels:  $E_S$  and  $M_e$  values for different cumulative  $P$ -wave windows. The diamonds mark the end of the  $P$ -wave windows that have been used for the single station  $M_e$  estimates. All the panels have the same scale values.

values of  $M_e$ , namely  $M_e$ (GFZ) 7.19 and 6.75, or  $M_e$ (USGS) 7.4 and 6.68 for the Costa Rica and Nicaragua earthquake, respectively.

### The 2007 September 13 and the 2007 October 24 Southern Sumatra earthquakes

In 2007 September–October, the Sumatra arc was affected by a number of moderate to major events after the great Bengkulu earthquake of 2007 September 12. Here we consider two earthquakes that occurred in Southern Sumatra with similar GCMT moment magnitudes, namely 7.0 for the 2007 September 13 and 6.8 for the 2007 October 24 earthquake, respectively. Their epicentre locations differed by about 250 km. Fig. 11 shows in the upper map the distribution of stations used in the analysis for both earthquakes (28 are in common), and next to the map cut-out below their almost identical GCMT fault plane solutions. Fig. 12 compares the records and analysis results for the station GNI, which is further away from the two earthquakes ( $65.4^\circ$  and  $67.6^\circ$ , respectively) than in the previous two examples of Figs 8 and 10. Despite their similarity in focal mechanism and seismic moment the two earthquakes differ in their  $M_e$  by about 0.7 m.u. and accordingly in their energy release by more than a factor of 10 ( $M_e$ (GFZ) 7.17 and 6.44 or  $M_e$ (USGS) 6.96 and 6.20 for the 2007 September 13 and the 2007 October 24 event, respectively). The time-frequency analyses show that the two events have similar low frequency ( $f < 0.1$  Hz) amplitudes (consistent with the similar  $M_0$  and  $M_w$ ), but the high-frequency part of

the spectra are very different. The first earthquake has much larger spectral amplitudes at frequencies between 0.1 and 0.3 Hz than the second one. This explains the significant differences in the equally scaled recordings. Moreover, the energy released by the first event is dominated by three energy pulses. The first one, lasting for about 20 s, arrives about 15 s after the first  $P$ -wave onset with dominating frequencies between 0.1 and 0.2 Hz. Soon after, a short second pulse (about 5 s long) and a third pulse between  $\sim 47$  and 70 s after the first  $P$ -wave onset arrive, both with  $f \sim 0.3$  Hz (unfortunately, due to the lack of studies regarding the rupture process of this event, a link between these energy pulses with the rupture process, as discussed in the case of the Costa Rica event, cannot be yet made).

In contrast, the second earthquake radiates its energy more homogeneously all over the rupture time, and this difference with respect to the first event is also obvious in the more gradual increase of the cumulative energy curve (compare the two lowermost panels of Fig. 12). Thus, this example illustrates also the large range of variability in the energy release by earthquakes with very similar mechanisms and occurring even in the same seismotectonic environment.

### CONCLUSIONS

We applied offline our rapid procedure to a large record data set of 767 earthquakes and proved the possibility to obtain  $M_e$  within 10–15 min after OT. The earthquakes have been classified by their GCMT fault plane solutions according to Zoback (1992). This step

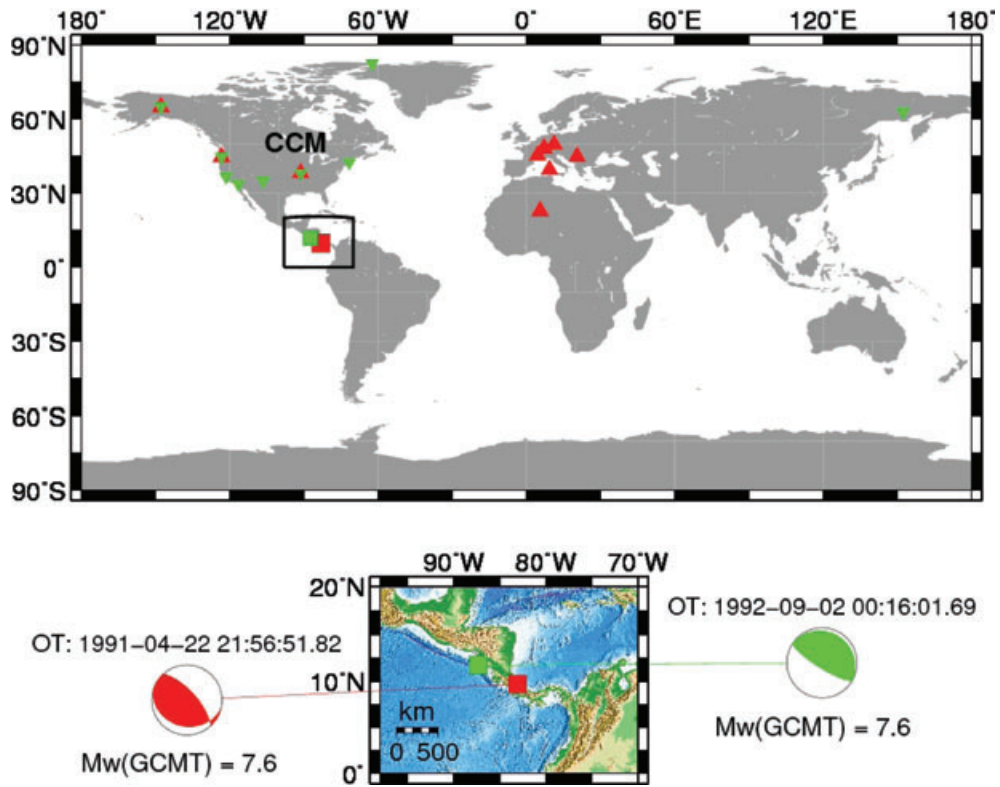


**Figure 9.** The upper map shows the locations of the two Central America earthquakes and the stations used to calculate  $Me(GFZ)$ . The red triangles represent the stations used for the earthquake of 1991 April 22, and the inverted green triangles for the event of 1992 September 2. The station CCM will be considered in the comparison of Fig. 10. The box delimitates the area shown enlarged in the lower map together with the GCMT fault plane solutions and related  $M_w$ .

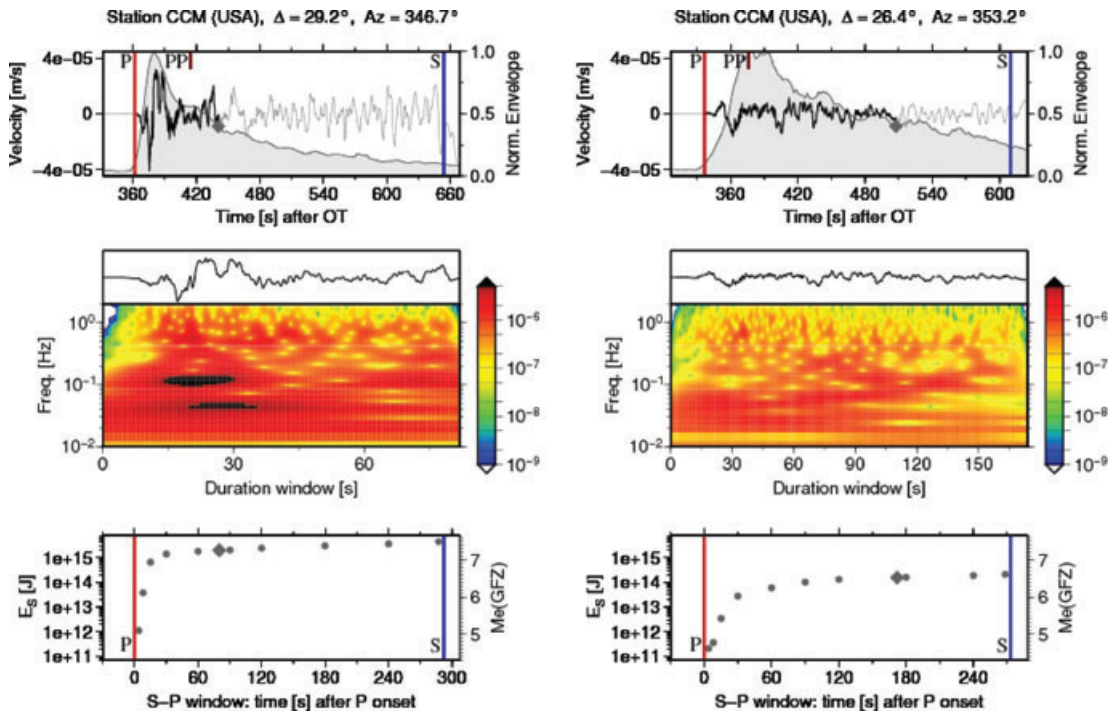


**Figure 10.** The same as for Fig. 8 at the station CCM (USA). The panels on the left-hand side refer to the Costa Rica earthquake of 1991 April 22 and the panels on the right-hand side to the Nicaragua earthquake of 1992 September 2.

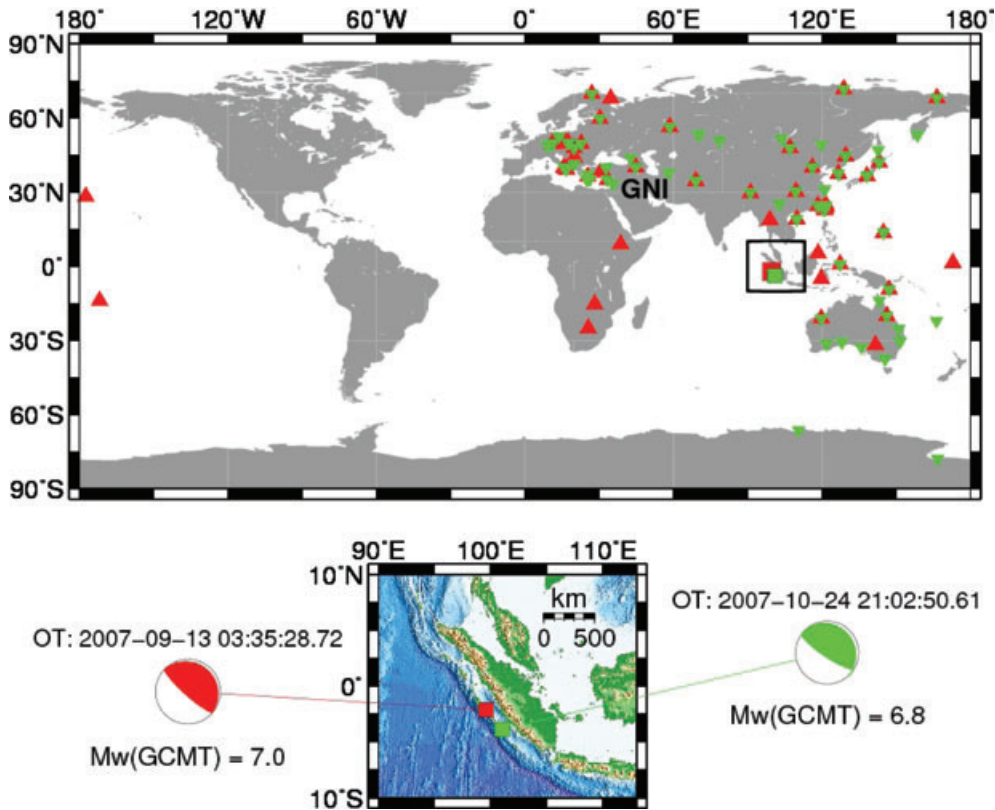


**Figure 11.** The upper map shows the location of the two analysed Southern Sumatra earthquakes and the stations used to calculate  $M_e(\text{GFZ})$ . The red triangles relate to stations used for the earthquake on 2007 September 13, and the inverted green triangles to stations used for the event on 2007 October 24. The station GNI will be considered in the comparison of Fig. 12. The box delimitates the area shown enlarged in the lower map together with the GCMT fault plane solutions and related  $M_w$ .

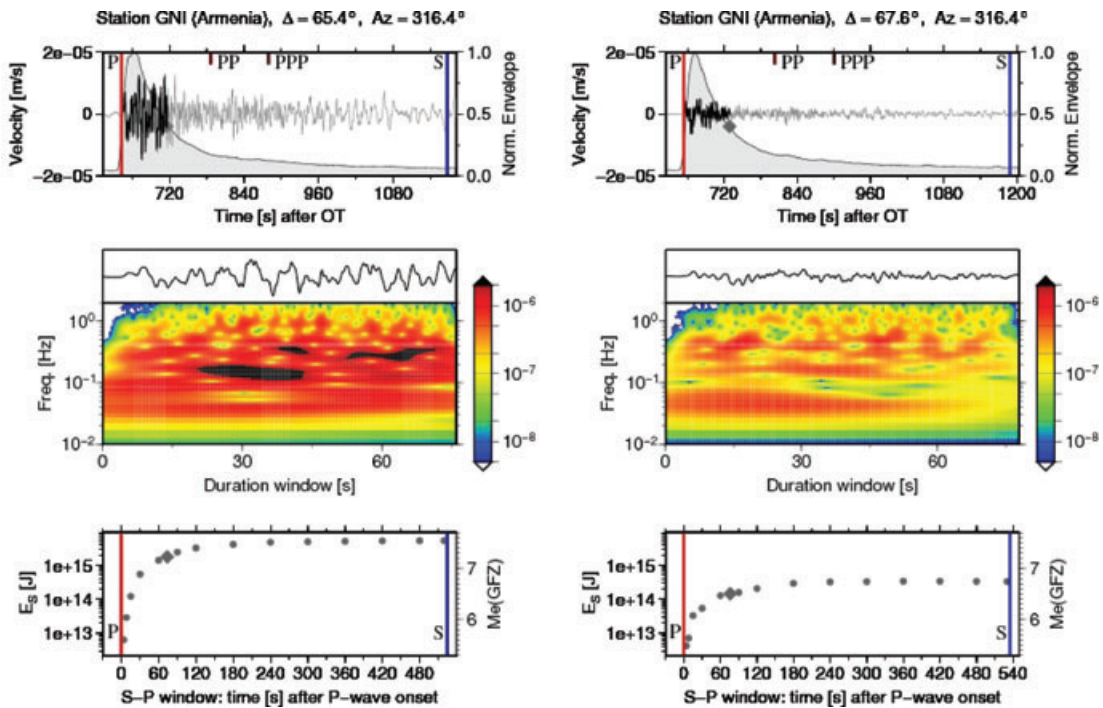


**Figure 12.** The same as for Fig. 8 at the station GNI (Armenia). The panels on the left-hand side refer to the Sumatra earthquake that occurred on 2007 September 13, and the panels on the right-hand side to the other Sumatra earthquake on 2007 October 24. In the uppermost panels also the theoretical PPP arrivals are marked.

has been performed in order to discuss possible effects of the focal mechanism on the Me determinations since we do not apply focal-specific corrections as the USGS does to obtain Me. According to our results, the rapid Me(GFZ) agrees with Me(USGS) within  $\pm 0.3$  m.u. for  $\sim 67$  per cent of the analysed events. This is satisfactory for a near real-time procedure. The largest discrepancies are observed for strike-slip events, for which Me(USGS) is almost systematically larger than Me(GFZ) and also larger than Mw(GCMT). This suggests that Me(USGS) values strongly depend on focal mechanism corrections for strike-slip earthquakes. This has already been noted by previous studies. In this context it has to be stressed that none of the classical magnitude procedures, to which also Mw and Me have been scaled (see Bormann *et al.* 2009), foresees *a priori* corrections of the measured amplitudes depending on the source mechanism. This may explain why our uncorrected Me values scale more linear and with less scatter than Me(USGS) with Mw(GCMT). These differences in the GFZ and USGS Me procedures notwithstanding, the comparisons between Mw(GCMT) and Me(USGS), as well as between Me(GFZ) with Mw from GCMT and USGS, have clearly shown that Mw and Me data complement each other well. Mw better represents the static properties of the source (e.g. the overall final displacement and rupture area), which are fundamental for assessing the earthquake's tsunamigenic potential, whereas Me is more suitable to quantify the fraction of energy involved in the rupture process that is transformed into seismic waves. Knowledge of the latter, however, is important for better assessing the shaking potential of an earthquake. Therefore, rapid and sufficiently accurate Me determinations are a useful complement to Mw and can help disaster management organizations to assess faster and more reliably the potential earthquake impact. This has been illustrated by way of example for six earthquakes that have been pairwise closely spaced in three different seismotectonic regions, with similar Mw but very different Me. Since the propagation paths for the respective event pairs are almost identical, the differences in the observed spectral contents can be attributed mainly to differences in source dynamics. It has been shown that the energy magnitude Me is sensitive to the relative amount of more high-frequency energy radiated by the seismic source, in contrast to Mw, that is controlled by the asymptotic low-frequency amplitudes only. Moreover, it has also been shown that even earthquakes with very similar focal mechanism and seismic moment occurring in the same seismotectonic area may radiate significantly different amounts of seismic energy. This highlights the need to introduce joint rapid routine measurements of both Mw and Me in global seismic monitoring practice.

## ACKNOWLEDGMENTS

This paper is part of the EU-SAFER project, contract number 036935. The authors would like to thank two anonymous reviewers for their valuable suggestions, which significantly improved the manuscript. Figures were drawn using the Generic Mapping Tool (GMT, Wessel & Smith 1991) software. Kevin Fleming kindly improved our English. The scientific research presented in this publication has been given financial support by the European Center for Geodynamics and Seismology, Luxembourg.

## REFERENCES

- Ammon, C.J., Kanamori, H. & Lay, T., 2008. A great earthquake doublet and seismic stress transfer cycle in the central Kuril islands, *Nature*, **451**, 561–U4, doi:10.1038/nature06521.
- Beresnev, I., 2009. The reality of the scaling law of earthquake-source spectra? *J. Seism.*, **13**, 433–436, doi:10.1007/s10950-008-9136-9.
- Bird, P., 2003. An updated digital model of plate boundaries, *Geochem. Geophys. Geosyst.*, **4**(3), 1027, doi:10.1029/2001GC000252.
- Boatwright, J. & Choy, G.L., 1986. Teleseismic estimates of the radiated energy by shallow earthquakes, *J. geophys. Res.*, **91**(B2), 2095–2112.
- Boatwright, J. & Fletcher, J.B., 1984. The partition of radiated energy between P and S waves, *Bull. seism. Soc. Am.*, **74**(2), 361–376.
- Bormann, P. & Saul, J., 2008. The new IASPEI standard broadband magnitude  $m_B$ , *Seism. Res. Lett.*, **79**(5), 699–705.
- Bormann, P. & Saul, J., 2009. A fast, non-saturating magnitude estimator for great earthquakes, *Seism. Res. Lett.*, **80**(5), 808–816, doi:10.1785/gssrl.80.5.808.
- Bormann, P., Baumbach, M., Bock, G., Grosser, H., Choy, G.L. & Boatwright, J., 2002. Seismic sources and source parameters, in *IASPEI New Manual of Seismological Observatory Practice*, Vol. 1, Chapter 3, pp. 94, ed. Bormann, P., Geoforschungszentrum, Potsdam.
- Bormann, P., Liu, R., Ren, X., Gutendutsch, R., Kaiser, D. & Castellaro, S., 2007. Chinese National Network magnitudes, their relation to NEIC magnitudes, and recommendations for the new IASPEI magnitude standards, *Bull. seism. Soc. Am.*, **97**, 114–127, doi:10.1785/0120060078.
- Bormann, P., Liu, R., Xu, Z., Ren, K., Zhang, L. & Wendt, S., 2009. First application of the new IASPEI teleseismic magnitude standards to data of the China National Seismographic Network, *Bull. seism. Soc. Am.*, **99**(3), 1868–1891, doi:10.1785/0120080010.
- Choy, G.L. & Boatwright, J., 1995. Global patterns of radiated seismic energy and apparent stress, *J. geophys. Res.*, **100**(B9), 18 205–18 228.
- Choy, G.L. & Boatwright, J., 2007. The energy radiated by the 26 December 2004 Sumatra–Andaman earthquake estimated from 10-minute P-wave windows, *Bull. seism. Soc. Am.*, **97**, S18–S24.
- Choy, G.L. & Kirby, S., 2004. Apparent stress, fault maturity and seismic hazard for normal-fault earthquakes at subduction zones, *Geophys. J. Int.*, **159**, 991–1012.
- Choy, G.L., Kirby, S. & Boatwright, J., 2006. An overview of the global variability in radiated energy and apparent stress, in *Earthquakes: Radiated Energy and the Physics of Faulting*, Vol. 170, pp. 43–57, eds Abercrombie, R. *et al.*, Geophysical Monograph Series.
- Di Giacomo, D., Grosser, H., Parolai, S., Bormann, P. & Wang, R., 2008. Rapid determination of Me for strong to great shallow earthquakes, *Geophys. Res. Lett.*, **35**, L10308, doi:10.1029/2008GL033505.
- Gilbert, F. & Backus, G., 1968. Elastic-gravitational vibrations of a radially stratified sphere, in *Dynamics of Stratified Solids*, pp. 82–95, ed. Hermann, G., Am. Soc. Mech. Eng., New York, NY.
- Goes, S.D.B., Velasco, A.A., Schwartz, S.Y. & Lay, T., 1993. The April 22, 1991, Valle de la Estrella, Costa Rica ( $M_w = 7.7$ ) earthquake and its tectonic implications: a broadband seismic study, *J. geophys. Res.*, **98**(B5), 8127–8142.
- Hanks, T.C. & Kanamori, H., 1979. A moment magnitude scale, *J. geophys. Res.*, **84**(B5), 2348–2350.
- Haskell, N.A., 1964. Total energy and energy spectral density of elastic wave radiation from propagating faults, *Bull. seism. Soc. Am.*, **54**(6), 1811–1841.
- Kanamori, H., 1977. The energy release in great earthquakes, *J. geophys. Res.*, **82**(20), 2981–2987.
- Kanamori, H., 1983. Magnitude scale and quantification of earthquakes, *Tectonophysics*, **93**, 185–199.
- Kanamori, H. & Kikuchi, M., 1993. The 1992 Nicaragua earthquake: a slow tsunami earthquake associated with subducted sediments, *Nature*, **361**, 714–716.
- Kanamori, H. & Rivera, L., 2008. Source inversion of W phase: speeding up seismic tsunami warning, *Geophys. J. Int.*, **175**, 222–238.
- Kennett, B.L.N., Engdahl, E.R. & Buland, R., 1995. Constraints on seismic velocities in the Earth from traveltimes, *Geophys. J. Int.*, **122**, 108–124.
- Lomax, A. & Michelini, A., 2009.  $M_{wpd}$ : a duration-amplitude procedure for rapid determination of earthquake magnitude and tsunamigenic potential from P waveforms, *Geophys. J. Int.*, **176**, 200–214, doi:10.1111/j.1365-246X.2008.03974.x.

- Lomax, A., Michelini, A. & Piatanesi, A., 2007. An energy-duration procedure for rapid and accurate determination of earthquake magnitude and tsunamigenic potential, *Geophys. J. Int.*, **170**, 1195–1209, doi:10.1111/j.1365-246X.2007.03469.x.
- Montagner, J.-P. & Kennett, B.L.N., 1996. How to reconcile body-wave and normal-mode reference Earth models? *Geophys. J. Int.*, **125**, 229–248.
- Newman, A.V. & Okal, E.A., 1998. Teleseismic estimates of radiated seismic energy: the  $E/M_0$  discriminant for tsunami earthquakes, *J. geophys. Res.*, **103**(B11), 26 885–26 898.
- Okal, E.A. & Talandier, J., 1989.  $M_m$ : a variable-period mantle magnitude, *J. geophys. Res.*, **94**(B4), 4169–4193.
- Parolai, S., 2009. Denoising of seismograms using the  $S$  transform, *Bull. seism. Soc. Am.*, **99**(1), 226–234, doi:10.1785/0120080001.
- Pérez-Campos, X. & Beroza, G.C., 2001. An apparent mechanism dependence of radiated seismic energy, *J. geophys. Res.*, **106**(B6), 11 127–11 136.
- Polet, J. & Thio, H.K., 2003. The 1994 Java tsunami earthquake and its “normal” aftershocks, *Geophys. Res. Lett.*, **30**(9), 1474, doi:10.1029/2002GL01686.
- Purcaru, G. & Berckhemer, H., 1978. A magnitude scale for very large earthquakes, *Tectonophysics*, **49**, 189–198.
- Rudnicki, J.W. & Freund, L.B., 1981. On energy radiation from seismic sources, *Bull. seism. Soc. Am.*, **71**(3), 583–595.
- Schweitzer, J. & Kværna, T. 1999. Influence of source radiation patterns on globally observed short-period magnitude estimates (mb), *Bull. seism. Soc. Am.*, **89**(2), 342–347.
- Stockwell, R.G., Mansinha, L. & Lowe, R.P., 1996. Localization of the complex spectrum: the  $S$  transform, *IEEE Trans. Signal Process.*, **44**, 998–1001.
- Sipkin, S.A., 1994. Rapid determination of global moment-tensor solutions, *Geophys. Res. Lett.*, **21**, 1667–1670.
- Tsuboi, S., Abe, K., Takano, K. & Yamanaka, Y., 1995. Rapid determination of  $M_w$  from broadband  $P$  waveforms, *Bull. seism. Soc. Am.*, **85**(2), 606–613.
- Vassiliou, M.S. & Kanamori, H., 1982. The energy release in earthquakes, *Bull. seism. Soc. Am.*, **72**(2), 371–387.
- Venkataraman, A. & Kanamori, H., 2004a. Effect of directivity on estimates of radiated seismic energy, *J. geophys. Res.*, **109**, B04301, doi:10.1029/2003JB002548.
- Venkataraman, A. & Kanamori, H., 2004b. Observational constraints on the fracture energy of subduction zone earthquakes, *J. geophys. Res.*, **109**, B05302, doi:10.1029/2003JB002549.
- Wang, R., 1999. A simple orthonormalization method for stable and efficient computation of Green’s functions, *Bull. seism. Soc. Am.*, **89**(3), 733–741.
- Weinstein, S.A. & Okal, E.A., 2005. The mantle magnitude  $M_m$  and the slowness parameter  $\Theta$ : five years of real-time use in the context of tsunami warning, *Bull. seism. Soc. Am.*, **95**(3), 779–799, doi:10.1785/0120040112.
- Wessel, P. & Smith, W.H.F., 1991. Free software helps map and display data, *EOS, Trans. Am. Geophys. Un.*, **72**(41), 441, 445–446.
- Zoback, M.L., 1992. First- and second-order patterns of stress in the lithosphere: the World Stress Map project, *J. geophys. Res.*, **97**(B8), 11 703–11 728.

## SUPPORTING INFORMATION

Additional Supporting Information may be found in the online version of this article;

**Table A1.** List of earthquake parameters for the events analyzed in this work.

Please note: Wiley-Blackwell are not responsible for the content or functionality of any supporting materials supplied by the authors. Any queries (other than missing material) should be directed to the corresponding author for the article.